

Comparative analysis for meaningful interpretation of rare-earth oxide $M_{4,5}$ energy loss edges

ELLIS KENNEDY¹, CHRISTINA CHOI², M.C. SCOTT^{1,2} *

¹Department of Materials Science and Engineering, University of California Berkeley, Berkeley, California, 94720, USA

²NCEM, Molecular Foundry, Lawrence Berkeley National Laboratory, Berkeley, California, 94720, USA

January 19, 2021

Abstract

The magnetic, electronic, and optical properties of rare earth-oxides are directly influenced by the valency of the metallic cation. With the development of next generation electron energy-loss spectrometers, high-energy lanthanide fine structure can be studied with improved signal-to-noise for quantitative analysis. Unfortunately, the behavior of rare-earth 4f orbital electrons is not well understood. To establish best practices for analysis of energy-loss spectra from lanthanide oxides, we have performed a comparative study of the four traditional white line analysis methods extended to lanthanide $M_{4,5}$ edges resulting from $3d \rightarrow 4f$ orbital transitions using data from Gatan's EELS Atlas. The M_4/M_5 spectral feature ratios were examined as a function of 4f occupancy. The M_4/M_5 spectral feature ratio decreases exponentially as 4f occupancy increases, except for a plateau between Sm^{3+} and Dy^{3+} . The full-width at half the maximum intensity of the M_4 edges shows increased broadening for Sm^{3+} through Dy^{3+} . We suggest that the plateau results from 4f-orbital half-filling and is explained through the relationship between electron transition probability and transition lifetime as expressed through Fermi's Golden Rule. Of the four spectral analysis methods described, only the integrated area method can be ascribed a quantitative physical interpretation.

INTRODUCTION

Sharp ionization peaks known as “white lines” are some of the most distinctive and useful features in the core-loss region of electron energy-loss spectroscopy (EELS). These edges result from the excitation of $2p$ core electrons to unoccupied d-states near the Fermi level in the transition metals and the excitation of $3d$ electrons to f-states near the Fermi level in the RE elements [1, 2, 3]. The sharp edges aid in the determination of chemical species and analysis of their electron valencies. The $L_{2,3}$ white lines visible in transition metal spectra are well documented [4, 5, 1, 6, 7] and many methods for edge analysis are presented across the literature [8, 5, 9]. However, information on the $M_{4,5}$ white lines present in RE spectra is sparse and generalized due challenges collecting high resolution spectral data in the high-energy EELS regime [10].

The emergence of next generation EELS spectrometers that can better detect high-loss energy edges with improved signal-to-noise will enable improved spectral collection [11, 12]. The commercialization of these spectrometers grants opportunity for in-depth analysis of near-edge fine structure in the high-loss regime. In anticipation of improved acquisition of high-loss EELS spectra that include RE $M_{4,5}$ edges, the extension of analytical techniques used for $L_{2,3}$ quantification to RE $M_{4,5}$ edges must be evaluated. A robust method for measuring 4f occupancy is beneficial for understanding the unique properties of binary RE oxides.

While $L_{2,3}$ white line ratios are used for determining the valency of transition metal ions [4, 13], the relationship between valency and edge geometry requires further theoretical work [14]. The valency of RE ions in binary oxides is often even more difficult to determine and influenced by the initial electron state degeneracy [15, 1]. Multiple valencies can exist simultaneously in a single sample [16, 17, 18] and X-ray diffraction studies have shown that RE-oxides can be polyvalent or nonstoichiometric due to oxygen site vacancies [19, 1]. X-ray absorption (XAS) and X-ray photoelectron spectroscopy (XPS) studies conclude that $3d \rightarrow 4f$ initial electron energy multiplicity makes the complex structure of the RE series difficult to fully characterize. In XAS, only intensity from energy multiplets following dipole selection rules are visible, while in XPS all energy transition effects are visible [20, 21]. XAS studies on transition metals illustrate the need to account for crystal field splitting and cubic symmetries when focusing on electron-energy transition contributions to $L_{2,3}$ white lines [22]. While disparate, analogous spectral features are present in both x-ray methods and they can be analyzed following similar physical principles. Due to limited lanthanide EELS studies, attempts to reconcile EELS measurements with those of XAS and XPS have been limited.

The relationship between the transition of electrons to the unoccupied 4f-orbital and the magnetic, optical, and electronic properties of RE alloys often depend on RE valency [23, 24, 25]. Spectroscopic studies of RE alloys concentrate on the excitation of $3d$ core electrons to the 4f orbital

*mary.scott@berkeley.edu

($3d^{10}4f^n \rightarrow 3d^9 4f^{n+1}$), which is the origin of many of the desirable material properties of RE alloys [26, 1, 21].

To aid in future efforts to quantify RE EELS spectra and relate them to X-ray methods, we used data from the Gatan EELS Atlas to perform a comparative study of common white line analysis methods (Table 1) [27]. We focused on the limitations, sensitivities, and physical interpretations of each method. We compared the results of common analysis methods when applied to the lanthanides (Fig. 1). We denote the four methods, shown in Figure 2, as (1) integrated M₄/M₅ edge area ratio with step function subtraction, (2) M₄/M₅ edge height ratio, (3) M₄/M₅ edge height ratio with step function subtraction, and (4) M₄/M₅ edge second derivative ratio. Multiplicity of initial 3*d* electron energy states is accounted for in two of the methods with the subtraction of step function of height ratio 3:2 from the M₄ and M₅ edges, respectively. Of the four white line analysis methods, only method (1) provides information on the complexities of the energy-loss interactions that occur during a 3*d*→4*f* electron event. However, echoing conclusions from research on the L_{2,3} edges, we caution against deriving solid state interpretations from M_{4,5} white lines without a thorough analytical approach [28].

Element	RE-oxide	RE-ion valence number	Stoichiometric 4 <i>f</i> occupancy
La	La ₂ O ₃	3	0
Ce	CeO ₂	4	0
Pr	Pr ₆ O ₁₁	3.67	1.33
Nd	Nd ₂ O ₃	3	3
Sm	Sm ₂ O ₃	3	5
Eu	Eu ₂ O ₃	3	6
Gd	Gd ₂ O ₃	3	7
Tb	Tb ₂ O ₃	3	8
Dy	Dy ₂ O ₃	3	9
Ho	Ho ₂ O ₃	3	10
Er	Er ₂ O ₃	3	11
Tm	Tm ₂ O ₃	3	12
Yb	Yb ₂ O ₃	3	13

Table 1: RE elements with corresponding oxides, ion valence numbers, and 4*f*-electron occupancy

Through a comparison of the four white line analysis methods, we discuss the Sm-Dy plateau feature that is centered around Gd³⁺, which breaks the exponential decreasing trend for M₄/M₅ intensity as a function of 4*f*-occupancy. Previous lanthanide oxide EELS studies do not offer an explanation for the sudden increase in M₄/M₅ spin-orbit feature ratio [29]. The full width at half maximum intensity (FWHM) of

each M_{4,5} edge was measured and considered with regard to the physics governing electron transition lifetime. The loosely bound and delocalized nature of 4*f* electrons in the lanthanides allows them to more easily hybridize with states centered around oxygen atoms [30, 31]. The behavior of the 4*f*-valence electrons is not fully understood, complicating analysis of lanthanide EELS spectra. We attribute the Sm-Dy plateau to energy-minimizing half-filling of the 4*f* orbital and 5*d* hybridization leading up to and beyond the Gd³⁺ ion, which is expected to have a half-filled 4*f*-orbital. The Sm-Dy plateau is most prominent for method (1), the only method that reflects the probability distribution of an electron transition to an excited state.

MATERIALS AND METHODS

RE-oxide M_{4,5} white lines were obtained from the Gatan EELS Atlas. High-energy regime M_{4,5} data for elements 57-60 (La, Ce, Pr, Nd) and 62-70 (Sm, Eu, Gd, Tb, Dy, Ho, Er, Tm, Yb) were available (Table 1). The edges lie between 832 and 1576 eV for this subset of the lanthanides. Data for Pm, which lacks a stable oxide, was absent. The same spectral data for each RE element were analyzed using four methods described in literature on white line analysis. We assumed negligible plural scattering since all spectra report a ratio of inelastic energy-loss intensity to zero-loss peak intensity below 1.0. The $I_{inelastic}/I_{ZLP}$ ratio for each sample is reported in the Gatan EELS Atlas and included in the Supplemental information with thickness range calculations for each sample [32, 27]. Ideally, the EELS spectra would be deconvolved with the zero-loss peak, but the required data were unavailable and the samples were determined to be sufficiently thin. All serial EELS spectra were collected under the following experimental parameters: a 200 keV operating voltage, a 100 mrad collection semi-angle, 20-40 probe sweeps, and 20-30 ms dwell times [32].

A power law background subtraction was performed using the CSI Spectrum Analyzer plugin for ImageJ [33]. Background windows were 50 eV wide and ended at least 10 eV before the onset of the M₅ edge. For the M₄/M₅ edge second derivative ratio method, no background subtraction was applied because it yields similar results as when the background is correctly subtracted, making this method more robust against inaccurate background assignment.

We applied four methods used to quantify L_{2,3} white lines to the M_{4,5} edges of the lanthanide series. For each method, we observed the ratio between a specific M₄ and M₅ spectral edge feature as a function of 4*f* valence orbital filling in binary RE oxides. The methods are shown in Figure 2 and detailed in the Supplemental information. All EELS spectra were sourced from the online Gatan EELS Atlas and are shown in Figure 1 [32]. Table 1 includes the RE-oxides studied and their stoichiometric valencies and 4*f*-occupancies.

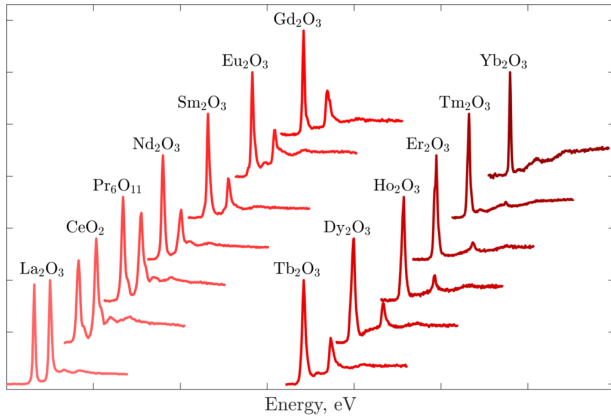


Figure 1: RE-oxide EELS spectra obtained from Gatan EELS Atlas and used to compare white line analysis methods [27]. Both axes are in arbitrary units as the figure is intended to show relative trends in M_4/M_5 edge feature ratio and in changing edge geometries with increasing RE Z-number and $4f$ -valency.

RESULTS

The four spectrum analysis methods produce the M_4/M_5 spin-orbit feature trends shown in Figure 3, in which the white line feature ratio is plotted as a function of $4f$ -orbital filling. The four methods are roughly in agreement. The lighter RE-oxides have larger M_4/M_5 white line feature ratios than the heavier lanthanides. M_4/M_5 feature ratios initially decrease, but with diminishing slope until reaching an inflection point at a $4f$ occupancy of approximately five electrons (Sm^{3+}). At this occupancy, the M_4/M_5 feature ratio increases across all methods. The trend then plateaus for methods (2) and (3). For methods (1) and (4), the trend reaches a second maxima at seven electron $4f$ occupancy (Gd^{3+}). The M_4/M_5 feature ratio begins to decrease again past a $4f$ occupancy of eight electrons. Overall, the feature intensity of the M_4 energy-loss edges is similar to that of the M_5 in the early lanthanides, but its relative intensity decreases rapidly toward the later lanthanides. This is also apparent in Figure 1.

Comparing the four methods, the M_4/M_5 feature ratio as a function of $4f$ -occupancy of method (1) deviates most significantly from the other three methods. The M_4/M_5 feature ratio for method (1) is, in general, higher than that for the other methods. The Sm-Dy plateau is most prominent when the data is analyzed with this method. There is a significant increase in the M_4/M_5 feature ratio centered about Gd^{3+} with seven electrons in the $4f$ -orbital. The other three methods display a less exaggerated Sm-Dy plateau centered at Gd^{3+} . As it is the integrated areas beneath white lines that relate to electron transition probability, method (1) is the only measurement with physical significance.

FWHM measurements of the $M_{4,5}$ white lines relate the energy spread of the white lines. FWHM values for the post-background subtraction $M_{4,5}$ edges are plotted in Figure 4. The M_4 edge FWHM decreases for RE-oxide ions with $4f$ -

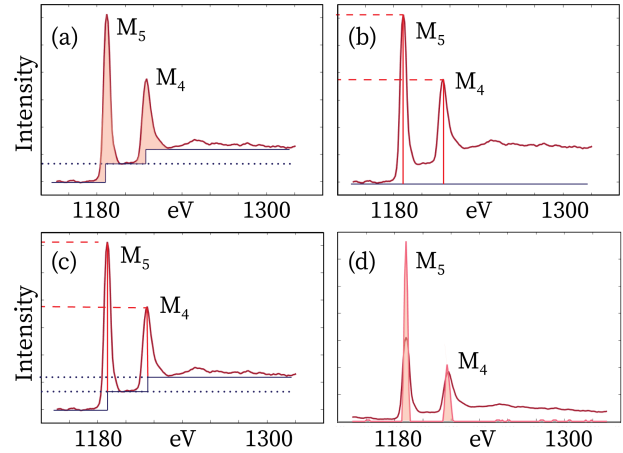


Figure 2: Illustration comparing the four methods of white line analysis that were used to study RE-oxide spectra. Gd^{3+} $M_{4,5}$ edges from a Gd_2O_3 sample are shown as representative white lines. (a) Method (1), integrated area ratio with step function subtraction with the area of each edge shaded in. (b) Method (2), height ratio with intensities indicated on the vertical axis with dashed red lines. (c) Method (3), height ratio with step area subtraction with the edge intensities indicated on the vertical axis with dashed red lines and the subtracted step values indicated with dotted lines. (d) Method (4), the positive component of the second derivative ratio is shown in pink with the integrated area for finding M_4/M_5 ratio shaded in. The second derivative plot is overlain on the Gd_2O_3 spectra without background fitting.

occupancies above that of $\text{Pr}^{3.67+}$ until reaching Eu^{3+} with six $4f$ electrons. There is a peak in the M_4 FWHM trend at Gd^{3+} , where the $4f$ -orbital is half-filled. The FWHM then decreases again until spiking at Er^{3+} with eleven $4f$ electrons.

Similar to the M_4 FWHM trend, the M_5 FWHM trend initially decreases for $4f$ -occupancies above that $\text{Pr}^{3.67+}$. Contrasting the trend in M_4 FWHM, the M_5 FWHM continues to decrease with a minimum at Gd^{3+} . Between Sm^{3+} and Dy^{3+} , the M_4 and M_5 FWHM trends are inverses, both with extrema centered at Gd^{3+} . The increase in area under the M_4 edge around Gd^{3+} and the accompanying decrease in area under the M_5 edge both contribute to the prominence of the Sm-Dy plateau shown in Figure 3, with the broadening likely attributable to $4f$ orbital half-filling. If significant multiple scattering were to occur it would disproportionately broaden the M_4 edge. However, because the ratio of inelastic energy-loss intensity to zero-loss peak intensity is below 1.0 for all spectra, the samples are sufficiently thin for plural scattering to be considered negligible [32].

DISCUSSION

Electron initial state multiplicity

Measured $M_{4,5}$ edges arise from a transition from an initial state in the d orbitals to a final state in the f orbitals. To

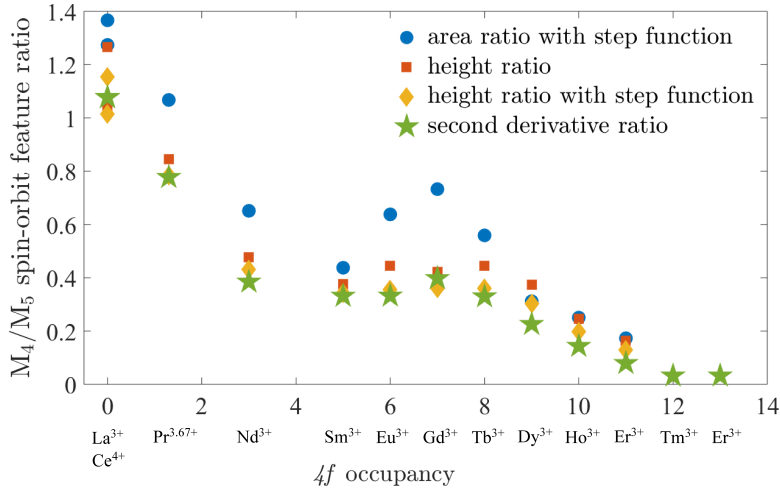


Figure 3: Dependence of the M_4/M_5 spin-orbit edge feature ratio on the stoichiometric electron occupancy of the $4f$ -orbital for the methods: (1) integrated edge area ratio with step function subtraction (blue circle), (2) edge height ratio (orange square), (3) edge height ratio with step function subtraction (yellow diamond), and (4) edge second derivative ratio (green star).

account for initial state electron multiplicity in this scenario, we extend the same physical principles of multiplicity used for analyzing $L_{2,3}$ edges to the $M_{4,5}$ edges because of similarities in electron exchange interactions and well-defined edge separation [34, 6, 14]. When this method has been applied to the $L_{2,3}$ transition metal white lines, the appropriate ratio of the step is 2:1, which correctly accounts for the multiplicity of the initial $2p$ electron states (four $2p^{3/2}$ and two $2p^{1/2}$). In theory, the step height ratio for the RE $M_{4,5}$ white lines is 3:2 because of the six initial $3d^{5/2}$ electron states and the four initial $3d^{3/2}$ electron states, as shown in Figure 5. The splitting of initial electron states results in the separate M_4 ($3d^{3/2} \rightarrow 4f^{5/2}$) and M_5 ($3d^{5/2} \rightarrow 4f^{7/2}$) edges observed in EELS [21]. In practice, the trough between the M_5 and M_4 edges often dips beneath the height of the lower step when the 3:2 ratio is applied from the continuum. When this happens, the energy at the nadir is taken as the height of the lower step. The step function is subtracted from the $M_{4,5}$ spectra for methods (1) and (3) with the implication that the energy multiplicity embedded in the continuum is accounted for.

Comparison of analysis methods

The four methods for EELS analysis under comparison have different sensitivity to spectral features in EELS data. Considerations for interpreting lanthanide EELS data analyzed using these methods are outlined in detail in the Supplemental information.

Physical interpretation of lanthanide EELS data

For $M_{4,5}$ transitions, the initial energy states are the $3d$ orbitals and the final states are the $4f$ orbitals. As indicated in Figure 5, the $3d^{3/2}$ initial energy state is of lower energy than the $3d^{5/2}$ initial state. An increasing M_4/M_5 ratio indicates that the energy-loss signal is increasingly composed of $3d^{3/2} \rightarrow 4f^{5/2}$ transitions. According to Hund's rule, unpaired electrons will fill available $4f$ orbitals first, with un-

paired electrons filling $4f^{7/2}$ orbitals beginning with Sm^{3+} . This corresponds to the first inflection point in Figure 4, as this represents when fewer final states begin to be available for the M_4 transition. This trend continues until Tb^{3+} , where electron pairs begin to form and fewer final states are available for the M_5 transition [35]. As the $4f$ orbitals are occupied, transitions to the lower energy $4f^{5/2}$ states are blocked by the Pauli exclusion principle and the loss spectra are dominated by excitations to the $4f^{7/2}$ states [36]. The empty, half full, and completely full states of the $4f$ -orbital provide the greatest energetic stability [37]. It is possible that to increase electron configuration stability, the trivalent RE ions of Sm^{3+} through Dy^{3+} have half filled or nearly half filled $4f$ -orbitals. The elements surrounding Gd^{3+} would also have approximately seven $4f$ electrons if this is the case and be partially $5d$ hybridized [30, 38].

If the trivalent RE ions adjacent to Gd^{3+} in Figure 3 all have nearly seven $4f$ -electrons, then the similarity in M_4/M_5 ratios between Sm^{3+} , Eu^{3+} , Gd^{3+} , Tb^{3+} , and Dy^{3+} is explained. However, this does not explain why the Sm-Dy plateau rises in the edge area ratio method. The $3d^{10}4f^n \rightarrow 3d^94f^{n+1}$ electron energy transition probability is governed by the density of available final states and the pathways to the final states. The M_4 Sm-Dy plateau white lines exhibit broadening and increased relative integrated areas compared to the trend observed in the rest of the lanthanides. Through Heisenberg's uncertainty principle, the increase in energy indicates lower mean transition lifetimes and higher transition probabilities and rates [36]. Fermi's Golden Rule describes the dependence of transition probability on density of final states and coupling between the final and initial states, and can explain the differences in the intensities of the $M_{4,5}$ spectral lines [39]. According to Fermi's rule, increased transition probabilities, and therefore increased integrated

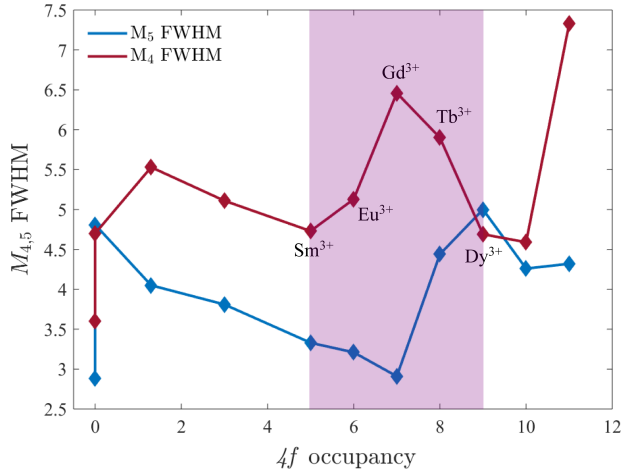


Figure 4: Measured FWHM of the M_4 (red) and M_5 (blue) edges for $4f$ -occupancies of elements 57-60 and 62-68. The FWHM of M_4 has a maximum at Gd^{3+} , the half-filled state. The FWHM of M_5 is minimized at Gd^{3+} . The shaded region is centered about a $4f$ -occupancy of seven electrons and indicates the RE oxides that contribute to the enhanced Sm-Dy plateau observed with method (1) in Figure 1.

area, should occur when more final states are available and coupling between states is higher.

An increase in the area under the M_4 edge is caused by a greater probability of electron transition to an excited state, which is indicative of an increase in the density of final states or in the accessibility of these final states. Stabilizing orbital half-filling increases both the density of final states and the transition pathways by offering more routes from initial state to final state. This indicates that the mean $4f$ occupancy is greater than stoichiometrically expected for Sm^{3+} and Eu^{3+} and less than expected for Tb^{3+} and Dy^{3+} . The M_5 Sm-Dy white lines exhibit reduced integrated areas, indicating reduced electron transition rates to $4f^{7/2}$ final states. The Sm-Dy plateau is not only explained by half-filling and hybridization, but is expected based on Fermi's rule.

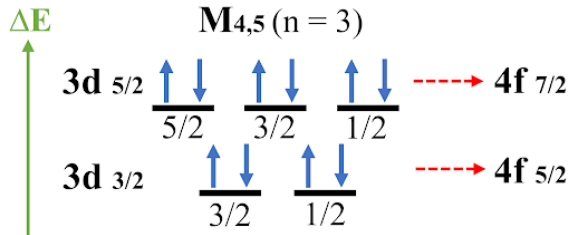


Figure 5: Spin orbit splitting diagram displaying the origin of $M_{4,5}$ edges and the 3:2 ratio of the $3d^{5/2}$ and $3d^{3/2}$ electron states.

Limitations in interpretation of EELS data for lanthanide oxides

The covalent character of RE-oxides limits the relationship between the cation oxidation state and the stoichiometric $4f$ - occupancy [28, 12]. There are additional limitations to

trusting stoichiometry and RE-oxygen atomic ratios may differ from those presented in Table 1. For example, La^{4+} and Ce^{3+} are both expected to have a $4f$ -orbital occupancy of zero electrons. Only the second derivative method results in the M_4/M_5 ratio of La^{4+} being slightly greater than that of Ce^{3+} . The other methods result in a greater M_4/M_5 ratio for Ce^{3+} , with the height ratio method resulting in the greatest difference. Studies have shown that RE-oxides often contain oxygen-site vacancies and that higher oxides, such as Pr_6O_{11} , frequently split into two or more polytypes in environmental conditions [40, 41]. The existence of multiple oxides within a single sample would be difficult to parse out in most $M_{4,5}$ EELS data, particularly if one oxide dominates. Modern advances in EELS detectors may assist by providing the resolution required to make out fine spectral features in the high energy-loss regime.

Additionally, the possibility of $4f$ - $4f$ electron energy transitions and $5d$ hybridization contributing to the shape of the plots in Figure 3 should also be considered. The Judd-Ofelt theory provides a theoretical framework for analyzing RE $4f$ - $4f$ electron energy transitions and outlined successive splitting of energy levels into many schemes of energy degeneracy [42, 43]. The energy splitting could influence the preferred $3d \rightarrow 4f$ transitions of energy-loss electrons, but is likely less significant than the effects of $4f$ half filling and $5d$ hybridization for energy minimization.

Ultimately, the EELS spectral features and plateau feature observed for M_4/M_5 feature ratios as a function of $4f$ -occupancy result from many factors, including ions stabilized with half-filled $4f$ orbitals, the presence of multiple oxides in a single sample, oxygen-vacancies resulting in nonstoichiometric compositions, and $5d$ hybridization. It seems likely that in a system with such complex electron interactions, more than one (if not all) of these properties will contribute to $M_{4,5}$ edge geometry in the lanthanides. Determining the weighted contributions of each requires furthering theoretical knowledge on $4f$ -electrons and collecting well-resolved EELS data from standard lanthanide oxides.

SUMMARY

In conclusion, we hope to offer insight for those performing EELS analysis on the lanthanide $M_{4,5}$ edges. We used four methods of white line analysis to plot M_4/M_5 spectral feature ratios as a function of $4f$ occupancy for lanthanide oxides. For two of the methods, we extended principles of initial state electron multiplicity by subtracting a 3:2 energy-loss intensity step-function from the M_5 and M_4 edges, respectively, to account for the broken degeneracy of $3d$ electron energies in a crystal field. There is a general decrease in M_4/M_5 feature intensity as the $4f$ fill level increases, but the Sm-Dy plateau emerges toward the half-fill point that is centered about Gd^{3+} . The Sm-Dy plateau is most evident

using method (1), indicating that the Sm-Dy plateau height is dependent on the area beneath the M_{4,5} edges. M₄ edge broadening responsible for the Sm-Dy plateau is attributed to 4*f* orbital half-filling, but is not fully understood, as electron itinerancy and 5*d* hybridization may contribute to the electron interactions responsible for this feature.

Of the four methods described, the integrated area method is the only method that provides quantitative information on M_{4,5} electron energy-loss behavior by incorporating the probability of electron transitions to excited states and the interactions of these excited states with other atomic states in the system. However, further theoretical development is required to explain edge geometry in terms of electron energy transitions and interactions and caution should be exercised when attributing electron-loss intensity to solid state effects. M_{4,5} white line analysis does not provide an accurate measurement of cation oxidation state, especially not for RE-oxides with sizeable covalent character [28]. Density functional theory calculations of lanthanide oxides with varying 4*f*-occupancy would help explain ground state transitions and 4*f* electron interactions responsible for the M_{4,5} edges observed with EELS. Those who desire simple fingerprinting can use the edge height method as it conveys a similar trend as the other methods and provides quick approximation, while the second derivative height ratio method provides analysis that is unbiased with respect to background. Researchers would benefit from updated, absolute-energy positioned RE-oxide spectra in the *EELS Atlas* and accompanying zero-loss peak data.

With the emergence of next generation direct-detection detectors, low signal-to noise high-energy regime EELS data can be collected from the lanthanide series. A theoretically-supported understanding of the experimentally observed energy-absorption and energy-loss features encoded in M_{4,5} EELS data would forward understanding of 4*f* electron behavior in the lanthanides.

ACKNOWLEDGMENTS

This work was supported by the National Science Foundation, DMR-1548924. Work at the Molecular Foundry was supported by the Office of Science, Office of Basic Energy Sciences, of the U.S. Department of Energy under Contract No. DE-AC02-05CH11231. We thank Liam Spillane at Gatan Inc. for providing information on the samples from which the spectra were collected. We thank Rohan Dhall at the Molecular Foundry, Lawrence Berkeley National Laboratory for enlightening conversations that influenced the direction of the work.

REFERENCES

- [1] T. Manoubi, C. Colliex, and P. Rez, “Quantitative electron energy loss spectroscopy on M₄₅ edges in rare earth oxides,” *Journal of Electron Spectroscopy and Related Phenomena*, vol. 50, no. 1, pp. 1–18, 1990. Publisher: Elsevier.
- [2] D. H. Pearson, B. Fultz, and C. C. Ahn, “Measurements of 3d state occupancy in transition metals using electron energy loss spectrometry,” *Applied Physics Letters*, vol. 53, pp. 1405–1407, Oct. 1988. Publisher: American Institute of Physics.
- [3] J. Zaanen, G. A. Sawatzky, J. Fink, W. Speier, and J. C. Fuggle, “L_{2,3} absorption spectra of the lighter 3d transition metals,” *Physical Review B*, vol. 32, pp. 4905–4913, Oct. 1985. Publisher: American Physical Society.
- [4] J. Graetz, C. C. Ahn, H. Ouyang, P. Rez, and B. Fultz, “White lines and d-band occupancy for the 3d transition-metal oxides and lithium transition-metal oxides,” *Physical Review B*, vol. 69, p. 235103, June 2004. Publisher: American Physical Society.
- [5] H. Kurata, E. Lefèvre, C. Colliex, and R. Brydson, “Electron-energy-loss near-edge structures in the oxygen K-edge spectra of transition-metal oxides,” *Physical Review B*, vol. 47, pp. 13763–13768, May 1993. Publisher: American Physical Society.
- [6] D. H. Pearson, C. C. Ahn, and B. Fultz, “White lines and d-electron occupancies for the 3d and 4d transition metals,” *Physical Review B*, vol. 47, pp. 8471–8478, Apr. 1993. Publisher: American Physical Society.
- [7] L. Yedra, E. Xuriguera, M. Estrader, A. López-Ortega, M. D. Baró, J. Nogués, M. Roldan, M. Varela, S. Estradé, and F. Peiró, “Oxide Wizard: An EELS Application to Characterize the White Lines of Transition Metal Edges,” *Microscopy and Microanalysis*, vol. 20, pp. 698–705, June 2014. Publisher: Cambridge University Press.
- [8] G. A. Botton, C. C. Appel, A. Horsewell, and W. M. Stobbs, “Quantification of the EELS near-edge structures to study Mn doping in oxides,” *Journal of Microscopy*, vol. 180, no. 3, pp. 211–216, 1995.
- [9] T. Riedl, T. Gemming, and K. Wetzig, “Extraction of EELS white-line intensities of manganese compounds: Methods, accuracy, and valence sensitivity,” *Ultramicroscopy*, vol. 106, pp. 284–291, Mar. 2006.
- [10] I. MacLaren, K. J. Annand, C. Black, and A. J. Craven, “EELS at very high energy losses,” *Microscopy*, vol. 67, pp. i78–i85, Mar. 2018.
- [11] J. L. Hart, A. C. Lang, A. C. Leff, P. Longo, C. Trevor, R. D. Twosten, and M. L. Taheri, “Direct Detection Electron Energy-Loss Spectroscopy: A Method to Push

- the Limits of Resolution and Sensitivity,” *Scientific Reports*, vol. 7, Aug. 2017.
- [12] I. MacLaren, R. B. Cummings, F. Gordon, E. Frutos-Myro, S. McFadzean, A. P. Brown, and A. J. Craven, “Chapter Twelve - Performing EELS at higher energy losses at both 80 and 200 kV,” in *Advances in Imaging and Electron Physics* (P. W. Hawkes and M. Hÿtch, eds.), vol. 210 of *Advances in Imaging and Electron Physics*, pp. 299–355, Elsevier, Jan. 2019.
- [13] J. Yuan, T. Hirayama, Y. Ikuhara, and T. Sakuma, “Electron energy loss spectroscopy study of cerium stabilised zirconia: an application of valence determination in rare earth systems,” *Micron*, vol. 30, pp. 141–145, Apr. 1999.
- [14] n. Wang, n. Yin, and n. Jiang, “EELS analysis of cation valence states and oxygen vacancies in magnetic oxides,” *Micron (Oxford, England: 1993)*, vol. 31, pp. 571–580, Oct. 2000.
- [15] M. Gasgnier, G. Schiffmacher, P. Caro, and L. Eyring, “The formation of rare earth oxides far from equilibrium,” *Journal of the Less Common Metals*, vol. 116, pp. 31–42, Feb. 1986.
- [16] S.-i. Kimura, F. Arai, and M. Ikezawa, “Mixed valence of praseodymium oxides,” in *Proceedings of the 11th International Conference on Vacuum Ultraviolet Radiation Physics* (T. Miyahara, Y. Azuma, M. Watanabe, and T. Ishii, eds.), pp. 135–138, Amsterdam: Elsevier, Jan. 1996.
- [17] N. F. Mott, “Rare-earth compounds with mixed valencies,” *The Philosophical Magazine: A Journal of Theoretical Experimental and Applied Physics*, vol. 30, pp. 403–416, Aug. 1974.
- [18] G. Sankar, P. R. Sarode, and C. N. R. Rao, “A XANES study of mixed-valence transition-metal oxides and rare-earth alloys,” *Chemical Physics*, vol. 76, pp. 435–442, May 1983.
- [19] Z. C. Kang and L. Eyring, “The prediction of the structure of members of the homologous series of the higher rare earth oxides,” *Journal of Alloys and Compounds*, vol. 275-277, pp. 30–36, July 1998.
- [20] G. Crecelius, G. K. Wertheim, and D. N. E. Buchanan, “Core-hole screening in lanthanide metals,” *Physical Review B*, vol. 18, pp. 6519–6524, Dec. 1978. Publisher: American Physical Society.
- [21] B. T. Thole, G. van der Laan, J. C. Fuggle, G. A. Sawatzky, R. C. Karnatak, and J.-M. Esteva, “3d x-ray-absorption lines and the $3d^9 4f^{n+1}$ multiplets of the lanthanides,” *Physical Review B*, vol. 32, pp. 5107–5118, Oct. 1985. Publisher: American Physical Society.
- [22] F. M. F. de Groot, J. C. Fuggle, B. T. Thole, and G. A. Sawatzky, “2p x-ray absorption of 3d transition-metal compounds: An atomic multiplet description including the crystal field,” *Physical Review B*, vol. 42, pp. 5459–5468, Sept. 1990. Publisher: American Physical Society.
- [23] J. R. Jeffries, K. T. Moore, N. P. Butch, and M. B. Maple, “Degree of 5f electron localization in URu₂Si₂: Electron energy-loss spectroscopy and spin-orbit sum rule analysis,” *Physical Review B*, vol. 82, p. 033103, July 2010. Publisher: American Physical Society.
- [24] T. Marcinow and K. Truszkowska, “Rare earth oxide films: their preparation and optical properties,” *Applied Optics*, vol. 20, pp. 1755–1757, May 1981. Publisher: Optical Society of America.
- [25] V. B. Shenoy and C. Rao, “Electronic phase separation and other novel phenomena and properties exhibited by mixed-valent rare-earth manganites and related materials,” *Philosophical Transactions of the Royal Society A: Mathematical, Physical and Engineering Sciences*, vol. 366, pp. 63–82, Jan. 2008. Publisher: Royal Society.
- [26] R. C. Karnatak, J. M. Esteva, and J. P. Connerade, “On the profiles and linewidths of the $3d \rightarrow 4f$ transitions in the lanthanides,” *Journal of Physics B: Atomic and Molecular Physics*, vol. 14, pp. 4747–4754, Dec. 1981. Publisher: IOP Publishing.
- [27] Gatan, “EELS Atlas.” EELS.info.
- [28] H. Tan, J. Verbeeck, A. Abakumov, and G. Van Tendeloo, “Oxidation state and chemical shift investigation in transition metal oxides by EELS,” *Ultramicroscopy*, vol. 116, pp. 24–33, May 2012.
- [29] J. A. Fortner and E. C. Buck, “The chemistry of the light rare-earth elements as determined by electron energy loss spectroscopy,” *Applied Physics Letters*, vol. 68, pp. 3817–3819, June 1996. Publisher: American Institute of Physics.
- [30] C.-G. Duan, T. Komesu, H.-K. Jeong, C. N. Borca, W.-G. Yin, J. Liu, W. N. Mei, P. A. Dowben, A. G. Petukhov, B. D. Schultz, and C. J. Palmstrøm, “HYBRIDIZATION BETWEEN 4f-5d STATES IN ErAs(100),” *Surface Review and Letters*, vol. 11, pp. 531–539, Dec. 2004. Publisher: World Scientific Publishing Co.
- [31] L. Zhang, J. Meng, F. Yao, X. Liu, J. Meng, and H. Zhang, “Strong-correlated behavior of 4 f electrons

- and 4 f 5 d hybridization in PrO₂,” *Scientific Reports*, vol. 8, p. 15995, Oct. 2018. Number: 1 Publisher: Nature Publishing Group.
- [32] C. C. Ahn and P. Rez, “Inner shell edge profiles in electron energy loss spectroscopy,” *Ultramicroscopy*, vol. 17, pp. 105–115, Jan. 1985.
- [33] P. Cueva, R. Hovden, J. A. Mundy, H. L. Xin, and D. A. Muller, “Data Processing for Atomic Resolution Electron Energy Loss Spectroscopy,” *Microscopy and Microanalysis*, vol. 18, pp. 667–675, Aug. 2012. Publisher: Cambridge University Press.
- [34] O. L. Krivanek and J. H. Paterson, “Elnes of 3d transition-metal oxides: I. Variations across the periodic table,” *Ultramicroscopy*, vol. 32, pp. 313–318, May 1990.
- [35] C. Benelli and D. Gatteschi, “Magnetism of Lanthanides in Molecular Materials with Transition-Metal Ions and Organic Radicals,” *Chemical Reviews*, vol. 102, pp. 2369–2388, June 2002.
- [36] D. Williams and C. Carter, *Transmission Electron Microscopy*. New York, New York: Springer Science, 2009.
- [37] R. J. Boyd, “A quantum mechanical explanation for Hund’s multiplicity rule,” *Nature*, vol. 310, pp. 480–481, Aug. 1984. Number: 5977 Publisher: Nature Publishing Group.
- [38] T. Komesu, H. K. Jeong, D. Wooton, Y. B. Losovyj, J. N. Crain, M. Bissen, F. J. Himpe, J. Petrosky, J. Tang, W. Wang, I. N. Yakovkin, and P. A. Dowben, “4f hybridization and band dispersion in gadolinium thin films and compounds,” *physica status solidi (b)*, vol. 246, no. 5, pp. 975–980, 2009.
- [39] E. Merzbacher, *Quantum Mechanics*. John Wiley & Sons, Jan. 1998.
- [40] G.-y. Adachi and N. Imanaka, “The Binary Rare Earth Oxides,” *Chemical Reviews*, vol. 98, pp. 1479–1514, June 1998.
- [41] M. W. Shafer, J. B. Torrance, and T. Penney, “Relationship of crystal growth parameters to the stoichiometry of EuO as determined by I.R. and conductivity measurements,” *Journal of Physics and Chemistry of Solids*, vol. 33, pp. 2251–IN1, Jan. 1972.
- [42] B. R. Judd, “Optical Absorption Intensities of Rare-Earth Ions,” *Physical Review*, vol. 127, pp. 750–761, Aug. 1962. Publisher: American Physical Society.
- [43] G. S. Ofelt, “Intensities of Crystal Spectra of Rare-Earth Ions,” *The Journal of Chemical Physics*, vol. 37, pp. 511–520, Aug. 1962. Publisher: American Institute of Physics.
- [44] J. M. Martin, B. Vacher, L. Ponsonnet, and V. Dupuis, “Chemical bond mapping of carbon by image-spectrum EELS in the second derivative mode,” *Ultramicroscopy*, vol. 65, pp. 229–238, Oct. 1996.
- [45] D. R. G. Mitchell and B. Schaffer, “Scripting-customised microscopy tools for Digital Micrograph™,” *Ultramicroscopy*, vol. 103, pp. 319–332, July 2005.

SUPPLEMENTAL INFORMATION

RE-oxide	$I_{inelastic}/I_{ZLP}$	Thickness in nm (80 nm imfp)	Thickness in nm (120 nm imfp)
La_2O_3	0.37	25.18	37.78
CeO_2	0.25	17.85	26.78
Pr_6O_{11}	0.63	39.09	58.63
Nd_2O_3	0.55	35.06	52.59
Sm_2O_3	0.20	14.59	21.88
Eu_2O_3	0.26	18.49	27.73
Gd_2O_3	0.73	43.85	65.77
Tb_2O_3	0.78	46.13	69.19
Dy_2O_3	0.50	32.44	48.66
Ho_2O_3	0.20	14.59	21.88
Er_2O_3	0.16	11.87	17.81
Tm_2O_3	0.41	27.49	41.23
Yb_2O_3	0.24	17.21	25.81

Table 2: Estimates of RE-oxide thickness based on lower (80 nm) and upper (120 nm) bounds of inelastic mean free path lengths (imfp) provided in the EELS Atlas (Ahn and Krivanek, 1983). All samples are thin films except Sm_2O_3 , which was in nanoparticle form.

Detailed description of methods for analyzing white line spectra

Method 1: Integrated area ratio with step function subtraction

Oxides of elements 57-60 and 62-68 were analyzed using the integrated edge area ratio with step function subtraction. Tm^{3+} and Yb^{3+} were excluded because significant M_4 edge broadening and reduced edge intensity made distinguishing the edge onset and shape from the background continuum subjective. After background subtraction, the data were normalized and a step function threshold was subtracted from the background. Using the method demonstrated by Pearson et al. 1988 [2], the white line intensity ratio was determined with consideration for the multiplicity of the initial $3d$ electron states. A horizontal line was fit over a range of 50 eV immediately following the M_4 white line.

A double step function was created from the horizontal line modeling the background continuum with the step onsets occurring at the M_4 and M_5 white line maxima eV values as shown in Figure 2(a) on a representative spectrum of the

Gd^{3+} $M_{4,5}$ edges. Edge onsets were selected using those listed in the EELS Atlas and edge ends were determined manually as the energy at which the edge intensity coalesces into the background intensity. The integrated area beneath the $M_{4,5}$ edges and above the step function, indicated by light shading in Figure 2(a), was used to determine the M_4/M_5 edge area ratio.

Method 2: Height ratio

A simple analysis of edge height ratio was performed on the same eleven RE-oxide samples. Like the L_2/L_3 edge height ratio, the M_4/M_5 edge height ratio is not generally considered a robust method for white line analysis because it fails to account for the range of transition energies present during ionization and assumes consistent white line width. It is used for oxide fingerprinting [28, 14]. This method is included for comparison against the other methods presented. For the eleven binary oxides analyzed, after background subtraction, the data were normalized and the relative maximum intensities, or edge heights, of the M_4 to the M_5 edges of each RE ion were calculated. This is shown in Figure 2(b) with the edge maxima marked on the vertical intensity axis.

Method 3: Height ratio with step function subtraction

To account for the effect of the multiplicity of the initial $3d$ electron states, we analyzed the edge height ratio after subtraction of a step function from each spectra. The step function subtraction procedure was the same as that carried out for determining the integrated area ratio. For the eleven binary oxides, after background subtraction, the data were normalized and a 3:2 step function was subtracted from the background. Then, the relative maximum intensities of the M_4 to the M_5 edges of each RE ion were calculated as shown in Figure 2(c). Similar to method (2), this method assumes consistent white line width and is included for comparison with the other methods.

Method 4: Second derivative ratio

Binary oxides of elements 57-60 (La, Ce, Pr, Nd) and 62-70 (Sm, Eu, Gd, Tb, Dy, Ho, Er, Tm, Yb) were analyzed using the edge second derivative ratio method. Unlike the other methods, this method does not require background subtraction because the positive components of the second derivative corresponding to the $M_{4,5}$ edges are pronounced and unlikely to be mistaken as part of the second derivative of the continuum [44]. We used D.R.G. Mitchell's script *Measure EELS Peak Intensities* (ver. 4, published Apr. 2020) [45] to perform the second derivative calculation and found a similar trend to Fortner and Buck in the M_4/M_5 spin-orbit feature ratio (their Figure 1) [29] with the inclusion of EELS Atlas data for La^{3+} , Ce^{4+} , and $Pr^{3,67+}$.

The second derivative method yielded distinguishable peaks for the M_4 and M_5 edges of all RE-oxides analyzed, including Tm and Yb. Figure 2(d) overlays Gd^{3+} $M_{4,5}$ edges and the positive components of the second derivative of the $M_{4,5}$ edges over the same energy-loss region. By preventing the potential for slight differences in manual selection

of the power law background window for subtraction and removing the need to approximate the edge onsets and ends, this method is robust against methodological inconsistencies. The integrated area of the M_4 and M_5 second derivative features, indicated by light shading in Figure 2(d), were used to compute the M_4/M_5 second derivative ratio.

Detailed comparison of differences observed trends in the M_4/M_5 spin-orbit feature vs. $4f$ -occupancy with respect to method of data analysis

Method 1: Integrated edge area ratio

The integrated edge area ratio, method (1), is sensitive to total integrated intensities of the $M_{4,5}$ electron energy loss within an energy range defined by the edge width. The step function subtraction accounts for the multiplicity of $3d$ energy transitions by removing portions of the energy continuum beneath each edge in proportion to the number of degenerate initial states of the $3d$ electrons. The M_4 edge maximum intensity decreases from left to right across the row. The M_4 becomes increasingly more difficult to separate from the background as the energy width increases and the edge height decreases. The FWHM measurements of the $M_{4,5}$ edges vary over the lanthanide oxides observed in this work. The trend of increased FWHM, indicating edge broadening, that is centered at Gd^{3+} explains the exaggerated plateau feature that is observed using method (1).

Method 2: Height ratio

Method (2) is the most straightforward and works well for fingerprinting when minimal plural scattering is evident in a spectrum. It is sensitive to the predominant electron energy-loss event, but does not account for the other similar electron energy-loss processes (the spread of the peak). When plural scattering is present, the M_4 edge height is increased more than the M_5 edge height. Because the multiplicity of the $3d104fn \rightarrow 3d94fn+1$ transitions are not considered with the subtraction of a 3:2 step function, the M_4 edge is favored. The effects of plural scattering and $3d$ electron degeneracy are not accounted for with this method, resulting in an over-assessment of the M_4 edge height relative to the M_5 edge height.

While method (2) does not account for energy level multiplicity, plural scattering, or a range of energy-loss events near that of the edge maxima, it does offer the benefit of simplicity. After background subtraction, the relative edge maxima can be measured and compared to those of known RE-oxides. The method also does not require approximation of edge onset and end. However, as RE-oxide's spectra remain relatively understudied, it is difficult to find standardized spectra for the various valencies of some of the RE-ions.

Despite the deficiencies of the method, as is evident in Figure 3, it should be noted that the edge height ratio trend as a function of $4f$ electron occupancy closely follows those of the edge height ratio with step function subtraction and

edge second derivative methods. Predictably, the M_4/M_5 values for the edge height ratio without step function subtraction are always slightly greater than those for the edge height ratio with step function subtraction method because the unaccounted for 3:2 ratio of initial electron states.

Method 3: Height ratio with step function subtraction

Method (3) is rarely used as the edge height ratio without step function subtraction allows for quicker RE-oxide fingerprinting. It has been included to show its similarity in trend with the other methods and for a comparison with the edge area method that also accounts for initial energy state multiplicity.

Both methods (2) and (3) show a plateau in M_4/M_5 feature ratio surrounding Gd^{3+} . However, these two methods also both indicate slight decrease in the M_4/M_5 feature ratio at Gd^{3+} itself. It is likely that the depression results from the methods being entirely insensitive to the energy spread of the edges. Figure 4 shows a sharp increase in the FWHM of the M_4 edge and a decrease in the FWHM of the M_5 edge of Gd^{3+} . The edge height with step function subtraction can be applied for fingerprinting and when only the predominant (most intense) $M_{4,5}$ energy-loss transitions are desired for analysis. Method (3) shows a trend similar to the edge second derivative method, but, by neglecting the energy spread of the edges, it does not provide any information on the complexities of the energy-loss interactions happening during a $3d \rightarrow 4f$ electron event.

Method 4: Second derivative ratio

Method (4) is performed independently of the confounding spectra contributions of plural scattering, $3d$ energy multiplicity, and the background energy continuum. This does not mean they are accounted for, just that they may be disregarded during analysis. It is the most robust method of calculating white line intensity ratios. It provides an easy method of fingerprinting white line spectra, but does not directly yield information on the energy spread of the electron. Because it is calculated from the rate of change of the slopes of the $M_{4,5}$ edges it includes some measure of spread, but not directly as the edge area ratio method does. The slope and geometry of the white lines influence the second derivative measurements. Beyond fingerprinting, this method is best applied when the M_4 and M_5 edges have similar slope and concavity. The M_4/M_5 trend as a function of $4f$ electron occupancy for method (4) closely follows that of method (3). The greatest deviation between the two occurs for the later trivalent RE ions where the second derivative yields a lower M_4/M_5 feature ratio.